Liquid leakage sensor with a V-shaped defect coupling structure based on polymer optical fibers

Jun Wang, Wanjia Gao, Yanjun Hu, Fei Li and Yanjun Zhang

Abstract—**In this study, a novel high-reliability liquid leakage sensor with a V-shaped defect coupling structure (VDCS) is proposed and experimentally demonstrated using polymer optical fibers (POFs) based on a light-emitting diode (LED) side-coupled light source. Liquid leakage detection is achieved with changes in the refractive index as the coupling medium transforms from air to liquid. The LED lamp both provides a light source and assists positioning. The coupling efficiency of the POF liquid leakage sensor varies with the depth and angle of the VDCS. Experimental results show that the coupling efficiency of the POF leakage sensor is high when the VDCS depth is 0.5 mm and the inclination angle is 60°. Compared to an existing leakage sensor with a hole-shape defect coupling structure (HDCS), the VDCS has a faster response time and higher reversibility. The average reliability of the liquid leakage sensor is increased to 5.92 μW/mL. This research provides a powerful structural reference for POF side-coupling leak measurement and can also be applied to the fields of gas and humidity sensing.**

Index Terms—**Fiber-optic sensing, Leak detection, Side coupling, Optical design.**

I. INTRODUCTION

LEAK detection has important applications in semiconductor factories and power facilities, among other locations. Common leak detection sensors employ the negative pressure wave method [1,2], sound signal analysis [3–6], and stress wave detection method [7–10]. Because of the cross-sensitivity of acoustic signals, these measurement methods are of limited efficacy in complex spaces. Optical fibers can be arranged in complex spatial structures and can resist electromagnetic interference, so their usage has received extensive attention [11–14].

At present, the principle guiding most optical fiber-based liquid leakage detection methods is the scattering of optical fibers (i.e., Raman, Brillouin, and Rayleigh) [15–20]. Optical frequency-domain reflectometry is used in long-distance detection [22,23]. It relies strongly on demodulation technology; however, demodulated signals are susceptible to interference from external conditions. Optical time-domain reflectometry detection technology uses single-mode optical fibers, handling single-mode optical fiber can be costly in terms of splicing and slicing tools as well as the complexity of introducing structures on the side [23,24]. In the existing sensors, the conversion of a liquid leakage event into a change in temperature or strain is time-consuming, which affects the real-time performance of the system. Special structures, such as cones [24] and gratings, can be machined on the fiber [15,16], which can improve the measurement accuracy of the sensor and reflect changes in the refractive index. However, such structural processing is complicated, which increases costs. Recent studies have proposed a cost-effective side-coupling method to process a hole-shape defect coupling structure (HDCS) on a multimode fiber that reflects leakage events through changes in the defect coupling structure of the medium. The light source of the system is a low-cost light-emitting diode (LED) lamp belt [25]. However, it is difficult to clear the leakage in the HCDS quickly, which affects the reversibility of the sensor. The coupling efficiency of the hole-shape structure is low, and the defect coupling structure requires further research.

In this paper, a polymer optical fiber (POF) leakage sensor with a V-shaped defect coupling structure (VDCS) is proposed. The sensor consists of a flexible lamp belt (FLB) with LEDs and a POF with a VDCS. The change in the medium's refractive index in the VDCS directly reflects the leakage event. The FLB assists in positioning. The sensor performances of HDCS and VDCS are compared through experiments. Experimental results show that the VDCS has an effective fiber side-coupling structure that provides a better solution for leak detection.

II. MATERIALS AND METHODS

A. Leak Location Method

In this experiment, the FLB is used to achieve accurate positioning. According to with the simulated testing environment in the laboratory, we set the spacing of LED lights to be 5 cm. The spacing of LED can be adjusted according to the actual application. These LEDs correspond to the positions

of the VDCSs on the POF. The positioning schematic of the POF liquid leakage sensor with the VDCS is shown in Fig. 1.
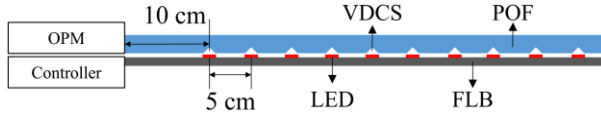

Fig. 1. Schematic of positioning.

Fig. 1 shows that the distance between the optical power meter (OPM) and the first VDCS processed on the POF is 10 cm. We created a coupling area by processing the side-coupling structure on the POF, and the emitted LED light was coupled into the core from the side of the POF [26].

The controller was used to control the specified LEDs. During the experiment, only one LED was turned on. The first LED was turned on for 1 s and then turned off, and then the second LED was turned on for 1 s and then turned off. This process was repeated until the last LED was turned on and off; the process then resumed with the first LED [25]. We recorded the power value displayed on the OPM when the LED was lighted. In the detection process, we set a threshold between leakage and watertight to achieve leakage detection. Because the lamp was controlled by a computer program, we could extract the position of the lamp from the program and combine the position of the lamp and output power to determine the location of the leakage.

B. Sensing Principle

The focus of this research is the component of light propagating in the vertical direction of the VDCS; our team previously examined light propagating in the horizontal direction of the HDCS [25]. The included angle of the VDCS is influential to the experimental results. In accordance with the principle of light propagation [27–30], assuming that the distance between the LED and the POF, d, was zero, the analysis results for VDCS included angles of 60° are shown in Fig. 2(a); those for included angles of 120° are shown in Fig. 2(b). Due to the limitations of experimental equipment, other parameter of the VDCS will be studied in our follow-up work.

The light emitted by the LED in Fig. 2 is confined to an angle by the silicone resin, which is represented as a red shaded part. When the medium in the VDCS is air, we assume that line *ABC* is the light at the critical position where total reflection occurs in the fiber and line *DEF* is the limiting light with a positive numerical aperture of the LED. Because the length of the VDCS is much greater than the wavelength of light, we did not consider the evanescent field effect [31]. Since the cladding thickness is much smaller than the fiber core diameter, the influence of the cladding refractive index is not considered. In this experiment, the liquid used for leakage testing is water.

In Fig. 2(a), the light *DEF* is used for demonstration analysis, the same principle apply to other lights in the LED's range of positive and negative numerical apertures. When the light beam reaches the critical surface of the organic resin and
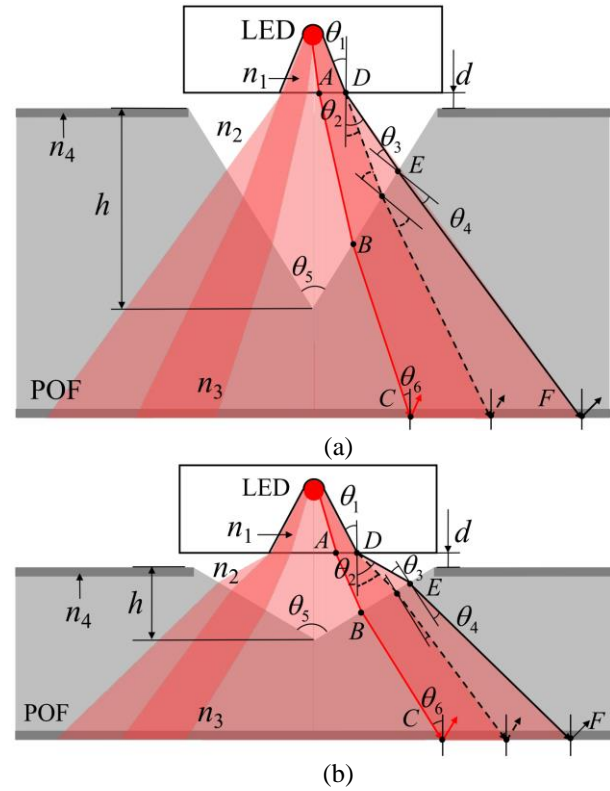

Fig. 2. Schematic of sensing principle: (**a**) Angle of VDCS is 60°; (**b**) Angle of VDCS is 120°.

air, the refraction point is marked as D. The beam reaches the inclined surface of the VDCS during the second refraction; this point is marked as E. At point D, according to Huygens' principle [32], the change in θ_2 can be obtained by Equation (1) [33]:

$$n_1 \cdot \sin \theta_1 = n_2 \cdot \sin \theta_2 \qquad (1)$$

where θ_1 is the incident angle of point D and θ_2 is the refraction angle. The refractive index of the silicone resin of the LED part is recorded as n_1 ($n_1 = 1.53$), and the refractive index of the gap coupling part of the VDCS is n_2. When the medium in the VDCS is air, n_2 is 1.00. When the medium in the VDCS is water, n_2 changes and is recorded as n_2' ($n_2' = 1.33$). The presence of water mainly affects the numerical aperture of the LED. The path of the light rays propagating along *DEF* has changed, which is represented by the black dashed line of Fig. 2(a). The results show that when the VDCS is filled with water, the refraction angle θ_2 decreases. At point E, the change in θ_3 can be obtained by Equation (2):

$$n_2 \cdot \sin \theta_3 = n_3 \cdot \sin \theta_4 \qquad (2)$$

where θ_3 is the incident angle and θ_4 is the refraction angle. The refractive index of POF is n_3 ($n_3 = 1.49$). The included angle of the VDCS is recorded as θ_5. The results show that when the VDCS is filled with water, the refraction angle θ_4 of point E increases. Through the analysis of geometric principles, we can get Equation (3):

$$\theta_4 = 90° - \theta_6 - \theta_5 / 2 \qquad (3)$$

where θ_6 is constant and θ_4 changes with θ_5. The change of θ_5 will cause the relative displacement of points B and E on the VDCS plane.

The analysis results for $\theta_5 = 120°$ are shown in Fig. 2(b), the analysis process is similar to the process for $\theta_5 = 60°$. Combining the above analysis, we assume a crude coupling efficiency, which is the partial solid angle emitted in the rays AB and DE divided by the total solid angle. The change of refractive index of VDCS medium affects the coupling efficiency and realizes leakage detection. In addition, the parameters of VDCS also affect the coupling efficiency. From the sensing principle, the proposed sensor is a general liquid leakage sensor.

C. Experimental Setup

The experimental devices include the sensing part, the control part, and an OPM (PDA200C, Thorlabs). The sensing part specifically includes a POF, a FLB, and a polyvinyl chloride (PVC) shell for fixing the POF and FLB. The core diameter of the multimode POF (SK80, Mitsubishi) selected in the experiment is 1960 μm. The FLB (CSO-DD-503, CSO Core Electronics) was controlled by a circuit board, and the control chip (SM16703P) was integrated inside the LED lamp. The core processor of the control part is the STM32F103RD chip, and the computer sends instructions to the controller, which then sends them to the LED. The optical signal output by the POF was converted into an electrical signal by a photodiode (SM05PD1A, Thorlabs). The OPM can measure the output signal of the POF with a resolution of 0.1 nW. The schematic of the experimental devices is shown in Fig. 3.
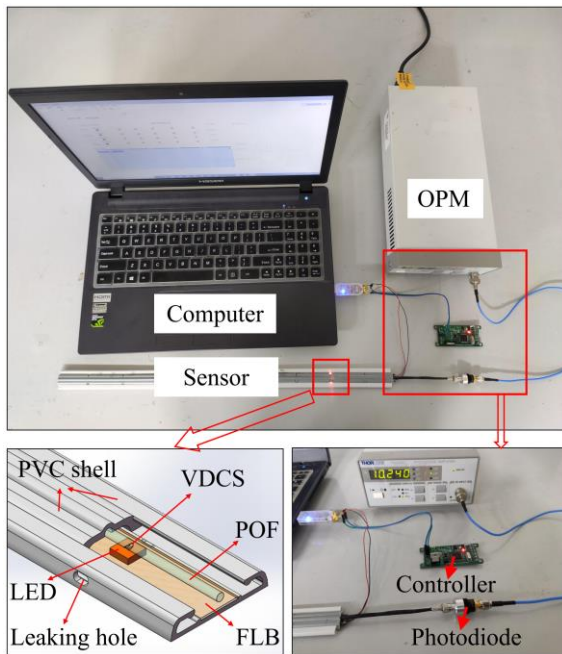

Fig. 3. Diagram of the experimental setup.

As shown in Fig. 3, the POF and FLB are fixed in the PVC shell structure. The VDCS was processed on the POF with a small computer numerical control machine tool to maintain consistency in the relative direction of the VDCS. The shell structure assembles the POF and LED lamp belt to ensure that each VDCS and the corresponding LED light are aligned to form a sensing unit. Compared with optical fiber fixed with tape, this simple shell structure increases the reliability of the experimental data. The light emitted by the LED lamp was coupled to the POF through the VDCS. The medium change between the VDCS and LED lamp caused the output light intensity to change. We used an OPM to measure the change in the output power at one end of the POF. The controller determined the LED's on/off status at a certain position on the FLB. Accordingly, the output power combined with the position of the LED enabled determination of the location of the liquid leakage. All experiments were performed at room temperature (20 ℃).

III. RESULTS

A. Optimal Parameter Selection of the VDCS

To ensure the accuracy of the experiments, we processed six sensor belts with a length of 60 cm. Nine VDCSs were processed on each sensor belt. The length of the POF was 60 cm, and the VDCS parameters of the six POFs are shown in Table I.

TABLE I
PARAMETERS OF SENSORS.

Symbol	Parameters of the VDCSs	
	Angle of θ_5	h (mm)
a		0.3
b	$\theta_5 = 60°$	0.4
c		0.5
d		0.3
e	$\theta_5 = 120°$	0.4
f		0.5

h: Depth of the VDCS

After all the equipment was assembled, we recorded the initial output power values of each point of the six sensors. We used a syringe to sequentially add 1 mL of water to each point and recorded the changes in the output power values. The next measurement was performed only when the water in the VDCSs was completely cleared away. The measurement was repeated 10 times, and the lowest value was recorded for comparison. The results of measuring the six sensors are shown in Fig. 4.

In Fig. 4, the black and red lines are the output power values with air and water, respectively. We regard the output power difference of the sensor with and without water as a manifestation of the pulse intensity. Greater pulse intensity, corresponds to a better experimental effect by the defect coupling structure. For $\theta_5 = 60°$, the pulse intensity of the sensor is high. For $\theta_5 = 120°$, the pulse intensity of the sensor is relatively low. As the depth h of the VDCS increases, the value of the output power also increases. Larger output power values correspond to stronger anti-interference ability in the sensor. We introduce a quality factor T, expressed as $T=(U_A-U_W)/U_A$, where U_A and U_W are the average output power
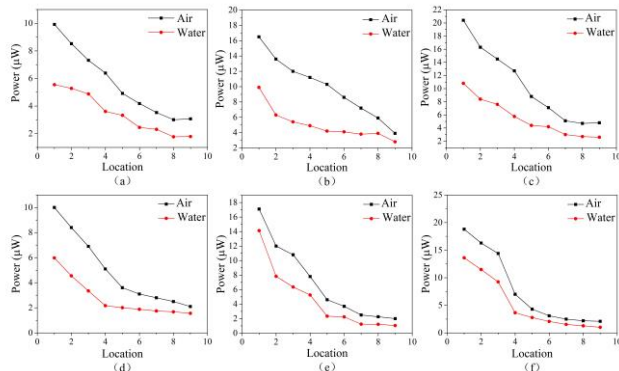
Fig. 4. Leakage liquid responses of different VDCSs: (**a**)–(**c**) Included angle of the VDCS is 60 ° and the depths are 0.3, 0.4, and 0.5 mm, respectively; (**d**)-(**f**) The included angle of the VDCS is 120 °and the depths are 0.3, 0.4, and 0.5 mm, respectively.

of air and water respectively. Based on this, the effect presented in Fig. 4(c) is the best. Correspondingly, when the depth is 0.5 mm and the angle θ_5 is 60 °, the performance of the VDCS is the best.

In processing VDCSs, measurement errors can occur due to human and instrument errors. In the future, we will consider using higher-precision equipment to process VDCSs. Nonetheless, the experimental results of the six sensors show that the output power decreases after adding water, which is consistent with the theoretical basis.

B. Reversibility and Response Time

We fabricated two sensing belts with a length of 115 cm. One is treated with VDCSs every 10 cm and the other was treated with HDCSs every 10 cm. We recorded the output power values without adding water as the initial values and then added 1 mL of water to the first leak hole using a syringe. To remove the water from the defect coupling structures, we blew the leaking hole with a simple pressure blower and recorded the recovery value as the stabilized output power. In recording the response time, for the first point on each sensor belt, the corresponding LED lamp was continuously kept on through circuit board control. The experimental results of response time are shown in the Fig. 5. The most of the water in the structure is blown away, but there is still some residual water which needs to be volatilized for a long time to be completely removed, so the recovery value recorded is a relatively stable value. The response time of holes in other positions is the same as that of the first hole, but the recovery value is different, the data results of the initial and recovery output power values recorded after many experiments are shown in Table II.
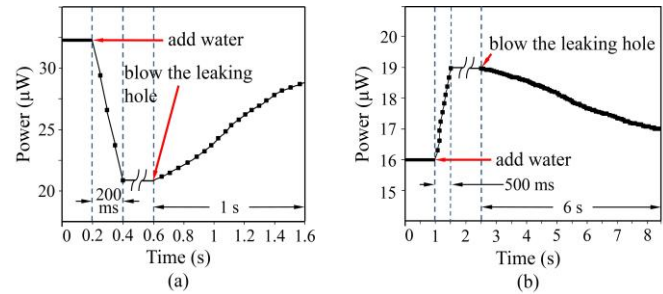

Fig. 5. Response times of sensors with different structures: (**a**) VDCS; (**b**) HDCS.

TABLE II
REVERSIBILITY TEST RESULTS.

Value	Sensing structure	1	2	3	4	5	6	7	8	9
x (µW)	VDCS	20.40	16.30	14.50	15.70	8.80	7.10	5.10	4.70	4.50
	HDCS	14.08	11.20	8.13	4.58	3.03	2.67	1.84	1.85	1.39
y (µW)	VDCS	18.53	15.52	13.27	14.15	8.13	6.82	4.74	4.24	4.20
	HDCS	17.75	13.62	9.87	6.00	3.92	3.27	2.33	2.35	1.76
z	VDCS	91%	95%	92%	90%	92%	96%	93%	90%	93%
	HDCS	74%	78%	79%	69%	71%	78%	73%	73%	73%

x: initial values; y: recovery values; z: values of the reversibility.

In Fig. 5(a), the time interval of the software data collection was 50 ms, so four collection points were obtained over 200 ms and the 20 total collection points were obtained in 1 s. Correspondingly, in Fig. 5(b), the response times of adding and removing water are 500 ms and 6 s, respectively. Therefore, the response time of the sensor with the VDCS is faster than that with the HDCS.

Table II shows that the recovery value of the HDCS is greater than the initial value, while that of the VDCS is smaller than the initial value. The value of z can be described by Equation (4):

$$z = \left(1 - \frac{|x - y|}{x}\right) \times 100\% \quad (4)$$

where x is the initial value and y is the recovery value. The recovery level is represented by z. A higher z value indicates better sensor reversibility. In Table II, the minimum z values of the VDCS and RCDS are 90% and 69%, respectively; the reversibility of the VDCS is clearly better than that of the HDCS.

C. Reliability

We processed two sensors with lengths of 115 cm. One sensor was processed with 20 VDCSs, where the distance between each pair of VDCSs was 5 cm. After selecting the parameters, the VDCS with the depth h of 0.5 mm and an angle of 60 ° was selected as the processing standard. The experimental results are shown in Fig. 6(a). The other sensor was processed with 20 HDCSs, where the distance between each pair of HDCSs was 5 cm. According to our previous research, the length, width, and height of the HDCSs were 3, 0.5, and 0.3 mm, respectively. The HDCS results are consistent

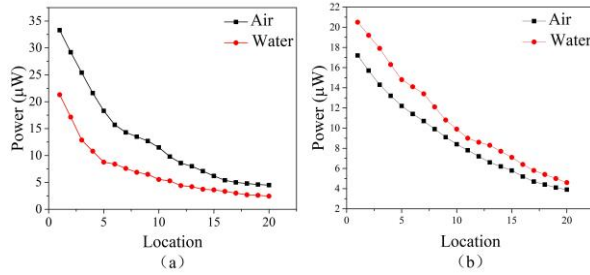with our previous results, and the experimental results are shown in Fig. 6(b).

Fig. 6. Reliability results of sensors with different structures: (**a**) VDCS; (**b**) HDCS

In Fig. 6, the black and red lines are the output power values in defect coupling structure media of air and water, respectively. According to the results in Fig. 6, the average of reliability Δv of VDCS and the average of reliability Δh of HDCS can be described by Equations (5) and (6), respectively:

$$\Delta v = \frac{\sum_{i=1}^{20} |a_{vi} - c_{vi}|}{20}, \quad (5)$$

$$\Delta h = \frac{\sum_{i=1}^{20} |a_{hi} - c_{hi}|}{20}, \quad (6)$$

where a_{vi} and a_{hi} are the output power values of the VDCS and HDCS when the medium is air, respectively, and c_{vi} and c_{hi} are the output power values of the VDCS and HDCS when the medium is water, respectively. The average reliability value reflects the reliability performance of the sensor. A higher average reliability indicates a higher- reliability sensor. Through calculations, we derive the value of Δv as 5.92 μW/mL and that of Δh as 1.95 μW/mL. Clearly, the reliability of the VDCS sensor is higher.

IV. CONCLUSIONS

This paper proposes a liquid leakage detection sensor based on a VDCS. The coupling method of this sensor uses the external light source of LED lamps. The fabrication process of the sensing structure is simple. The effects of the VDCS and HDCS on the sensor performances are compared through experiments. The final data show that when the depth of the VDCS is 0.5 mm and the angle is 60 °, the output pulse of the sensor probe is high. The response time of the liquid leakage sensor with the VDCS is faster than that with the HDCS. The reversibility of the VDCS is 90%, which is 21% higher than that of the HDCS. Within a measuring range of 1 m, the average reliability of the VDCS and HDCS are 5.92 and 1.95 μW/mL, respectively. The reliability of the VDCS is higher. The conclusions drawn in this experiment provide new ideas on the use of fiber side-coupling structures. Furthermore, through this experiment, we have a better understanding on the effects of

defect coupling structures on POF sensing, which provides a reference for the application of POF sensing in other fields.

REFERENCES

[1] X. Lang, P. Li, J. T. Cao, Y. Li, and H. Ren, "A Small Leak Localization Method for Oil Pipelines Based on Information Fusion," *IEEE Sensors Journal,* vol. 18, no. 99, pp. 6115-6122, 2018.
[2] P. Ostapkowicz, "Leak detection in liquid transmission pipelines using simplified pressure analysis techniques employing a minimum of standard and non-standard measuring devices," *Engineering Structures,* vol. 113, pp. 194-205, 2016.
[3] Y. Gao, M. J. Brennan, Y. Liu, F. C. L. Almeida, and P. F. Joseph, "Improving the shape of the cross-correlation function for leak detection in a plastic water distribution pipe using acoustic signals," *Applied Acoustics,* vol. 127, pp. 24-33, 2017.
[4] C. Yanlong, W. Weimin, G. Lei, S. Junjie, and L. Wuhua, "Numerical Simulation of the Pressure Gradient Method to Position Pipeline Leak," *Journal of Liaoning Shihua University,* 2014.
[5] J. Xu *et al.*, "Low-Cost, Tiny-Sized MEMS Hydrophone Sensor for Water Pipeline Leak Detection," *IEEE Transactions on Industrial Electronics,* vol. 66, no. 8, pp. 6374-6382, 2019.
[6] Butterfield *et al.*, "Prediction of leak flow rate in plastic water distribution pipes using vibro-acoustic measurements," *STRUCTURAL HEALTH MONITORING,* 2018.
[7] T. Li, J. Guo, Y. Tan, and Z. Zhou, "Recent Advances and Tendency in Fiber Bragg Grating-based Vibration Sensor: A Review," *IEEE Sensors Journal,* vol. PP, no. 99, pp. 1-1, 2020.
[8] X. Lang, P. Li, Y. Guo, J. Cao, and S. Lu, "A Multiple Leaks' Localization Method in a Pipeline Based on Change in the Sound Velocity," *IEEE Transactions on Instrumentation and Measurement,* vol. 69, no. 7, pp. 5010-5017, 2020.
[9] F. Okosun, P. Cahill, B. Hazra, and V. Pakrashi, "Vibration-based leak detection and monitoring of water pipes using output-only piezoelectric sensors," *The European Physical Journal Special Topics,* vol. 228, no. 7, pp. 1659-1675, 2019.
[10] Y. Chen, H. Sun, W. Zhang, and X. Huang, "Using stress wave technology for leakage detection in a landfill impervious layer," *Environ Sci Pollut Res Int,* vol. 26, no. 31, pp. 32050-32064, Nov 2019.
[11] Z. Liu *et al.*, "Spider silk-based tapered optical fiber for humidity sensing based on multimode interference," *Sensors and Actuators A: Physical,* vol. 313, 2020.
[12] Q. Wang, L. Han, X. Fan, and J. Zhu, "Distributed fiber optic vibration sensor based on polarization fading model for gas pipeline leakage testing experiment," *Journal of Low Frequency Noise, Vibration and Active Control,* vol. 37, no. 3, pp. 468-476, 2017.
[13] J. Zuo *et al.*, "Pipeline Leak Detection Technology Based on Distributed Optical Fiber Acoustic Sensing System," *IEEE Access,* vol. 8, pp. 30789-30796, 2020.
[14] N. Hayashi *et al.*, "Pilot demonstration of correlation-domain distributed temperature sensing using forward Brillouin scattering," *Japanese Journal of Applied Physics,* vol. 59, no. 8, 2020.
[15] M. Buric, K. P. Chen, M. Bhattarai, P. R. Swinehart, and M. Maklad, "Active Fiber Bragg Grating Hydrogen Sensors for All-Temperature Operation," *IEEE Photonics Technology Letters,* vol. 19, no. 5, pp. 255-257, 2007.
[16] J. R. Lee and H. Tsuda, "Fiber optic liquid leak detection technique with an ultrasonic actuator and a fiber Bragg grating," *Optics Letters,* vol. 30, no. 24, p. 3293, 2005.
[17] J. Li *et al.*, "High-accuracy distributed temperature measurement using difference sensitive-temperature compensation for Raman-based optical fiber sensing," *Opt Express,* vol. 27, no. 25, pp. 36183-36196, Dec 9 2019.
[18] Y. Shang, R. Guo, Y. Liu, and X. Yi, "Managing Brillouin frequency spacing for temperature measurement with Brillouin fiber laser sensor," *Optical and Quantum Electronics,* vol. 52, no. 4, 2020.
[19] Y. Muanenda, C. J. Oton, and F. Di Pasquale, "Application of Raman and Brillouin Scattering Phenomena in Distributed Optical Fiber Sensing," *Frontiers in Physics,* vol. 7, 2019.
[20] Y. Zheng, C. Chen, T. Liu, Y. Shao, and Y. Zhang, "Leakage detection and long-term monitoring in diaphragm wall joints using fiber Bragg grating sensing technology," *Tunnelling and Underground Space Technology,* vol. 98, 2020.

This article has been accepted for publication in a future issue of this journal, but has not been fully edited. Content may change prior to final publication. Citation information: DOI 10.1109/JPHOT.2021.3109801, IEEE Photonics Journal

> REPLACE THIS LINE WITH YOUR PAPER IDENTIFICATION NUMBER (DOUBLE-CLICK HERE TO EDIT) <   6

[21] J. Wang, L. Zhao, T. Liu, Z. Li, T. Sun, and K. T. V. Grattan, "Novel Negative Pressure Wave-Based Pipeline Leak Detection System Using Fiber Bragg Grating-Based Pressure Sensors," *Journal of Lightwave Technology,* vol. 35, no. 16, pp. 3366-3373, 2017.

[22] J. Li, X. Lu, and W. F. Wang, "Leak monitoring and localization in baghouse filtration system using a distributed optical fiber dynamic air pressure sensor," *Optical Fiber Technology,* vol. 57, 2020.

[23] Y. Xu *et al.*, "Pipeline Leak Detection Using Raman Distributed Fiber Sensor With Dynamic Threshold Identification Method," *IEEE Sensors Journal,* vol. 20, no. 14, pp. 7870-7877, 2020.

[24] W. H. Png, H. S. Lin, C. H. Pua, and F. A. Rahman, "Pipeline monitoring and leak detection using Loop integrated Mach Zehnder Interferometer optical fiber sensor," *Optical Fiber Technology,* vol. 46, pp. 221-225, 2018.

[25] Y. Zhang, Y. Hou, Y. Zhang, Y. Hu, and W. Liu, "A cost-effective quasi-distributed liquid leakage sensor based on the polymer optical fiber and flexible lamp belt with LEDs," *Optics Express,* vol. 26, no. 8, p. 10152, 2018.

[26] L. Htein, W. Fan, and W. T. Han, "Emission characteristics of the Yb3+-sensitized Tm3+-doped optical fiber upon pumping with infrared LED," *Journal of Luminescence,* vol. 145, pp. 198-201, 2014.

[27] T. Y. Hu and D. N. Wang, "Optical fiber in-line Mach-Zehnder interferometer based on dual internal mirrors formed by a hollow sphere pair," *Optics Letters,* vol. 38, no. 16, pp. 3036-3039, 2013.

[28] W. W. Li, W. P. Chen, D. N. Wang, Z. K. Wang, and X. Ben, "Fiber inline Mach–Zehnder interferometer based on femtosecond laser inscribed waveguides," *Optics Letters,* vol. 42, no. 21, p. 4438, 2017.

[29] Z. Yunfang, L. Chupao, L. Changrui, Y. Kaiming, L. Zhengyong, and W. Yiping, "Femtosecond laser-inscribed fiber interface Mach–Zehnder interferometer for temperature-insensitive refractive index measurement," *Optics Letters,* vol. 43, no. 18, pp. 4421-4424, 2018.

[30] D. Ethonlagi and M. Zavrsnik, "Fiber-optic microbend sensor structure," *Optics Letters,* vol. 22, no. 11, pp. 837-9, 1997.

[31] Y. Hu, A. Ghaffar, Y. Hou, W. Liu, F. Li, and J. Wang, "A Micro Structure POF Relative Humidity Sensor Modified With Agarose Based on Surface Plasmon Resonance and Evanescent Wave Loss," *Photonic Sensors,* 2020.

[32] M. R. Akram, C. He, and W. Zhu, "Bi-layer metasurface based on Huygens' principle for high gain antenna applications," *Opt Express,* vol. 28, no. 11, pp. 15844-15854, May 25 2020.

[33] A. Ritboon, "The effect of astigmatism induced by refraction on the orbital angular momentum of light," *Journal of Optics,* vol. 22, no. 7, 2020.

Yanjun Hu was born in Heilongjiang, China in 1991. She is a PhD candidate at the North University of China. She received her B.S. degree in School of instruments and electronics from North University of China in 2015.
Her current research interests include the study of optical fiber sensors for humidity, gas, and distributed measurements.

Fei Li Was born in Shanxi, China in 1995. She is a PhD candidate at the North University of China. She received her B.S. degree in School of physics and information engineering from Shanxi Normal University in 2016.
Her current research interests include the study of new high-speed data transmission bus.

Yanjun Zhang was born in Shanxi, China in 1975. He is an associate professor in the School of Instrument and Electronics at the North University of China. He is mainly engaged in teaching and researching in the field of measurement technology and instruments.
His current research interests include distributed data recording systems, wireless sensor networks, embedded systems, lossless compression coding, data encryption, multifunctional structure, special optical sensors, and new high-speed data transmission bus development work.

Jun Wang was born in Shanxi, China in 1995. He is a master student of North University of China. He received his M.S. degree in School of Instrument and Electronics from North University of China in 2020.
His current research interests include research on measurement technology and instruments.

Wanjia Gao was born in Shanxi, China in 1992. She is a PhD candidate at the North University of China. She received her B.S. degree in School of instruments and electronics from North University of China in 2015.
Her current research interests include the study of ultrasonic sensors for liquid level measurements.